Fractionation of Cl/Br during fluid phase separation in magmatic-hydrothermal fluids

Author(s):
Seo, Jung H.; Zajacz, Zoltán

Publication date:
2016-06

Permanent link:
https://doi.org/10.3929/ethz-b-000115910

Originally published in:
Geochimica et Cosmochimica Acta 183, https://doi.org/10.1016/j.gca.2016.04.009

This is the Green Open Access version of: Seo, J. H., Zajacz, Z., 2016. Fractionation of Cl/Br during fluid phase separation in magmatic-hydrothermal fluids. *Geochimica et Cosmochimica Acta, vol. 183, pp. 125-137.*
https://doi.org/10.1016/j.gca.2016.04.009

Fractionation of Cl/Br during fluid phase separation in magmatic-hydrothermal fluids

Jung Hun Seo [1, 2] **and Zoltán Zajacz** [2, 3]

[1] Department of Energy Resource Engineering, Inha University, Incheon, Korea

[2] Institute of Geochemistry and Petrology, ETH Zurich, 8092 Zurich, Switzerland

[3] Department of Earth Sciences, University of Toronto, Toronto, Canada

(e-mail) seo@inha.ac.kr

Abstract

Brine and vapor inclusions were synthesized to study Cl/Br fractionation during magmatic-hydrothermal fluid phase separation at 900 °C and pressures of 90, 120, and 150 MPa in Li / Na / K halide salt – H_2O systems. Laser ablation ICP-MS microanalysis of high-density brine inclusions show an elevated Cl/Br ratio compared to the coexisting low-density vapor inclusions. The degree of Cl/Br fractionation between vapor and brine is significantly dependent on the identity of the alkali metal in the system: stronger vapor partitioning of Br occurs in the Li halide – H_2O system compared to the systems of K and Na halide – H_2O. The effect of the identity of alkali-metals in the system is stronger compared to the effect of vapor-brine density contrast. We infer that competition between alkali-halide and alkali-OH complexes in high-temperature fluids might cause the Cl/Br fractionation, consistent with the observed molar imbalances of alkali metals compared to halides in the analyzed brine inclusions. Our experiments show that the identity of alkali metals controls the degrees of Cl/Br fractionation between the separating aqueous fluid phases at 900 °C, and suggest that a significant variability in the Cl/Br ratios of magmatic fluids can arise in Li-rich systems.

Keywords: Fluid Inclusions, Halogens, Phase Separation, Bromine, Chlorine

1. INTRODUCTION

Saline geologic fluids are important media for the transport of various metals, from basinal brines to active volcanoes and sites of ore deposition (Yardley, 2005; Balcone-Boissard et al., 2010; Lesne et al., 2011). Halogen systematics, notably the somewhat conservative Cl/Br ratio in saline hydrothermal fluids, have been considered to be an excellent tracers for the source of dissolved halides, recording large-scale physical-chemical processes in hydrothermal systems (Bohlke and Irwin, 1992a, b; Heinrich et al., 1993; Kesler et al., 1995; Kesler et al., 1996; Gleeson et al., 2001;

Wilkinson et al., 2005; Baker et al., 2008; Stoffell et al., 2008; Gleeson and Smith, 2009; Nahnybida et al., 2009; Seo et al., 2011). The Cl/Br ratio in seawater is homogeneous (mass ratio around 290) and suggested to be near-constant at least during the Phanerozoic (Channer et al., 1997; Foriel et al., 2004). The solubility behavior of metal chlorides and bromides in hydrothermal fluids is also similar, and only a few processes were proposed to lead to Cl/Br fractionation. These include selective incorporation of Cl in halide minerals during precipitation or re-dissolution (Braitsch, 1971), which has been suggested to be the dominant factor producing distinctly depleted or elevated Cl/Br ratios in basinal brines, including those forming Mississippi Valley-type Pb-Zn ore deposits (Kesler et al., 1995; Kesler et al., 1996; Heijlen et al., 2003; Muchez et al., 2005; Stoffell et al., 2008), and in fluids of sub-seafloor hydrothermal systems (Oosting and Von Damm, 1996; Berndt and Seyfried, 1997). In the case of magmatic-hydrothermal fluids, the incorporation of different halogen sources such as seawater and regional evaporites into the source magmas was suggested to yield the variability in Cl/Br ratios (Gleeson et al., 2001; Gleeson and Smith, 2009; Seo et al., 2011).

Another process proposed to be able to modify the Cl/Br ratios in hydrothermal fluids, is a density-dependent differential partitioning of Cl and Br during vapor-brine separation and phase segregation (Berndt and Seyfried, 1997; Von Damm et al., 2003; Liebscher et al., 2006; Foustoukos and Seyfried, 2007). This process was suggested based on modified Cl/Br ratios relative to the seawater in sub-seafloor hydrothermal fluids expelled at mid-ocean ridges (Oosting and Von Damm, 1996; Berndt and Seyfried, 1997; Von Damm et al., 2003). A few recent experimental studies have confirmed various degrees of Br and Cl partitioning during phase separation in hydrothermal fluids, but in contradictory directions. Autoclave experiments at 380–450 °C/22.9–41.7 MPa (Liebscher et al., 2006) and 400–550 °C/25.0–35.0 MPa (Foustoukos and Seyfried, 2007) in the NaCl-H_2O system were used to simulate the sub-seafloor hydrothermal environment. The results of Foustoukos and Seyfried (2007) indicate preferential Br partitioning into the low-salinity vapor phase fluids relative to the brines, consistent with natural observations (Von Damm et al., 2003). By contrast, otherwise similar experiments by Liebscher et al. (2006) at partly overlapping conditions reported elevated Cl/Br ratios in the vapor compared to the brine.

Experiments determining the degree of Br and Cl fractionation at much higher temperatures and pressures relevant to magmatic-hydrothermal and volcanic conditions are lacking. Here, we studied the vapor-brine partitioning of Br and Cl at high *P-T* of 900 °C/90, 120, 150 MPa in the KCl-KBr-H_2O, NaCl-NaBr-H_2O, and LiCl-LiBr-H_2O systems by using synthetic fluid inclusions. We examined the degree of halogen fractionation as a function of fluid density contrasts, and explored the effect of different alkali ions because K and Li can become significant or even dominant cations in high-temperature magmatic fluids (Audetat et al., 2008; Kouzmanov and Pokrovski, 2012). We synthesized coexisting low-density vapor and high-density brine inclusions using Molybdenum-Hafnium-Carbide (MHC) alloy pressure vessel assemblies, and subsequently measured the fluid inclusions by Laser Ablation Inductively Coupled Plasma Mass Spectrometry (LA-ICP-MS) using a dedicated analytical protocol for halogen determinations in singly-targeted fluid inclusions (Seo et al., 2011).

2. METHODS

2.1. Experimental Methods and Microthermometry

We synthesized coexisting high-density brine and low-density vapor inclusions (Fig. 1A) in various alkali chloride and alkali bromide-bearing aqueous systems using the rapid-quench Molybdenum-Hafnium-Carbide (MHC) alloy pressure vessel assemblies. The experimental temperature was 900 °C and Ar was used as pressure medium. The alkali ions include K (sample number #173), Na (#167, #169, and #170), and Li (#174) (Table 1). For the NaCl-NaBr-H_2O system, we used pressures of 90 MPa (#170), 120 MPa (#169), and 150 MPa (#167) to produce brine-vapor pairs with various density contrasts (Table 2). Experiments at 120 MPa were used to test the effect of the identity of alkali metals by comparing Na-, K- and Li-bearing systems. Doubly distilled water and high-purity KCl, KBr, NaCl, NaBr, LiCl, and LiBr were used for the preparation of starting solutions. A pre-fractured (PF) chip of inclusion-free quartz and an intact quartz chip for in-situ fracturing (IS) at run conditions were both loaded together with 40 mg of starting solutions of various compositions and sealed in deformable Au capsules. We also added 10-20 mg of dehydrated silica gel to promote a quartz fracture healing. The pre-fracturing of quartz was performed by heating the chips up to 700 °C and subsequently dropping them into cold distilled water. Coexisting brine and vapor phase fluids were successfully trapped in both pre-fractured (PF) and in-situ fractured (IS) quartz chips. The size of the brine inclusions was up to 50 μm in diameter, whereas vapor inclusions were generally smaller (up to 30 μm) (Fig. 1).

The mole fractions of dissolved salts in the starting solutions ($X_{salt}=X_{alkali\text{-}Cl} + X_{alkali\text{-}Br}$) ranged from $X_{salt}=0.010$ (or 3.14 wt%) to $X_{salt}=0.026$ (or 7.85 wt%), and the solutions were adjusted to be just slightly above the theoretical vapor salinity in the model NaCl-H_2O system at 90 MPa ($X_{salt}=0.005$ or 1.51 wt%), 120 MPa ($X_{salt}=0.010$ or 3.22 wt%), and 150 MPa ($X_{salt}=0.021$ or 6.45 wt%) at 900 °C as predicted by the algorithm of Driesner and Heinrich (2007) (Table 2 and Fig. 2). These relatively low starting salinities ensured high vapor to brine ratios at the experimental P-T. This minimizes brine contamination of the synthetic vapor inclusions, which is typically induced by heterogeneous entrapment of both fluid phases (Bodnar et al., 1985). In addition, it allows more precise estimation of Cl/Br in coexisting vapor inclusions by mass balance calculation, using only the Cl/Br ratios as analyzed in the brine inclusions and known for the starting solutions. The Cl/Br mass ratios in the starting solutions varied between 7.61 and 8.46 (Table 2). The solutions were significantly Br-enriched compared to natural geologic fluids (Cl/Br mass ratios of 25 - 5000; Heinrich et al., 1993) to enable more precise analysis of Br in the brine inclusions by LA-ICP-MS (Seo et al., 2011). The solvus in the NaCl-NaBr-H_2O, KCl-KBr-H_2O, and LiCl-LiBr-H_2O systems could potentially deviate from the model NaCl-H_2O system, however, we trapped high-density brine inclusions and low-density vapor inclusions in all experiments demonstrating the all employed starting fluid compositions fell into the two phase field of the respective systems (Fig. 1A). The density of the vapor phase was similar in all three systems as demonstrated by the similar vapor/liquid rations within the vapor inclusions at ambient temperature (Fig. 1B).

Microthermometry on the brine inclusions trapped in the *in situ* fractured quartz were conducted to obtain homogenization temperatures (T_h) and salt melting temperatures (Table 3). Note that because the fluids contain significant amounts of NaBr, KCl, KBr, LiCl, and LiBr, it is difficult to obtain salinities by the salt melting temperatures. However, the internal consistency of the

measured salt melting and homogenization temperatures can be used to check if vapor contamination of the brine inclusions may be significant. In addition, in the NaCl-NaBr-H_2O system, checking the T_h of the brine inclusions and comparing the data to those predicted for the NaCl-H_2O system by using the algorithm of Driesner and Heinrich (2007) provides an independent test on how closely the formation conditions of fluid inclusions match the nominal conditions of the pressure-vessel experiments, provided that the T_h of a brine inclusions (coexisting with vapor) represents their true trapping temperature. A Linkam TS-1500 heating stage at Inha University was used and the temperatures were calibrated with the melting temperatures of $K_2Cr_2O_7$ (398 °C), NaCl (801 °C), and Au (1064.2 °C).

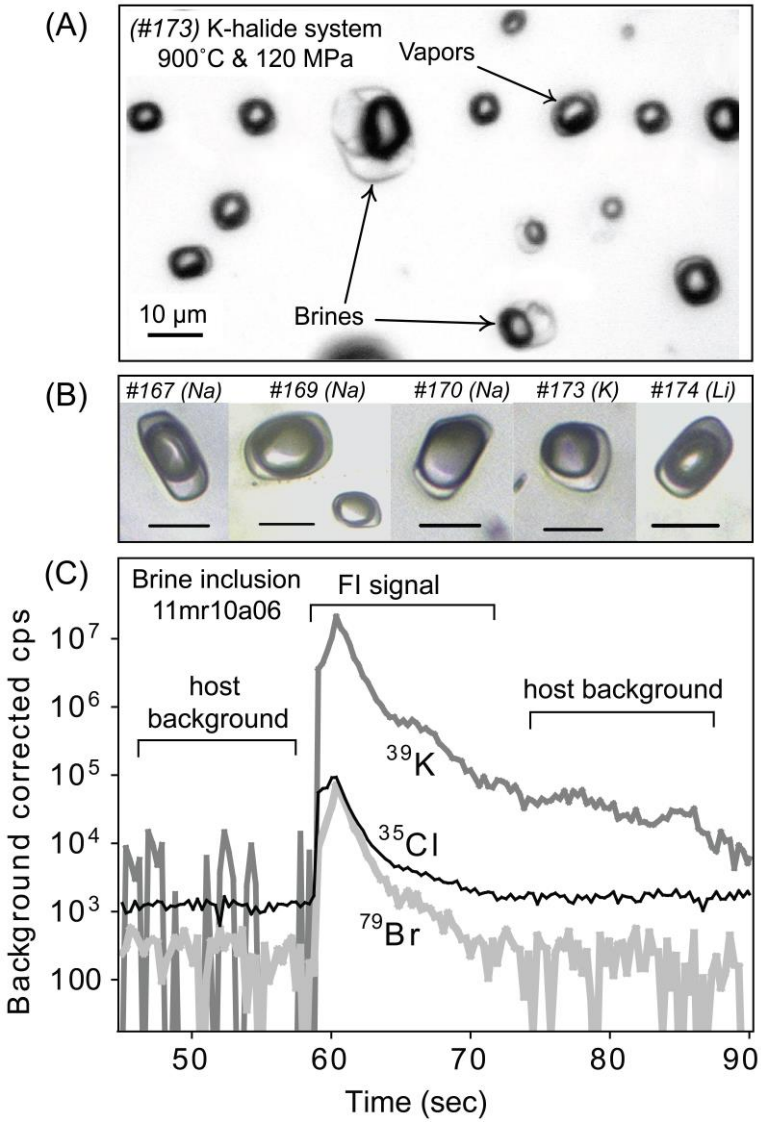

Figure 1. (A) Representative coexisting brine and vapor inclusions trapped by in-situ fracturing of quartz at 900 °C/ 120 MPa (#173 experiment). **(B)** Representative vapor inclusions trapped by in-situ fracturing of quartz. Volume % of the bubble in the #167, #169, #170, #173, and #174 vapor inclusions were estimated by petrographic analysis to be around 65-70 %, 75-80 %, 90%, 70-80 %, and 80 %, respectively. Vapor inclusions of #167 (Na-system), #169 (Na-system), and #170 (Na-system) conducted at different *P* conditions show different volume % of bubble indicating a different vapor density, while the vapor inclusions of #169 (Na-system), #173 (K-system), and #174 (Li-system) conducted at the same *P-T* condition show similar volume % of bubble. **(C)** LA-ICP-MS transient signal of a brine

inclusion produced in the K halide – H_2O system showing apparent peaks of K, Cl, and Br.

Table 1. Compositions of starting solutions and applied P-T conditions.

	#167	#169	#170	#173	#174
Alkali-Cl (molality)	1.33 (NaCl)	0.74 (NaCl)	0.51 (NaCl)	0.54 (KCl)	1.00 (LiCl)
Alkali-Br (molality)	0.08 (NaBr)	0.04 (NaBr)	0.03 (NaBr)	0.03 (KBr)	0.06 (LiBr)
Cl/Br (mass ratio)	7.61	7.80	7.80	8.46	8.06
P (Mpa)	150	120	90	120	120
T (°C)	900	900	900	900	900

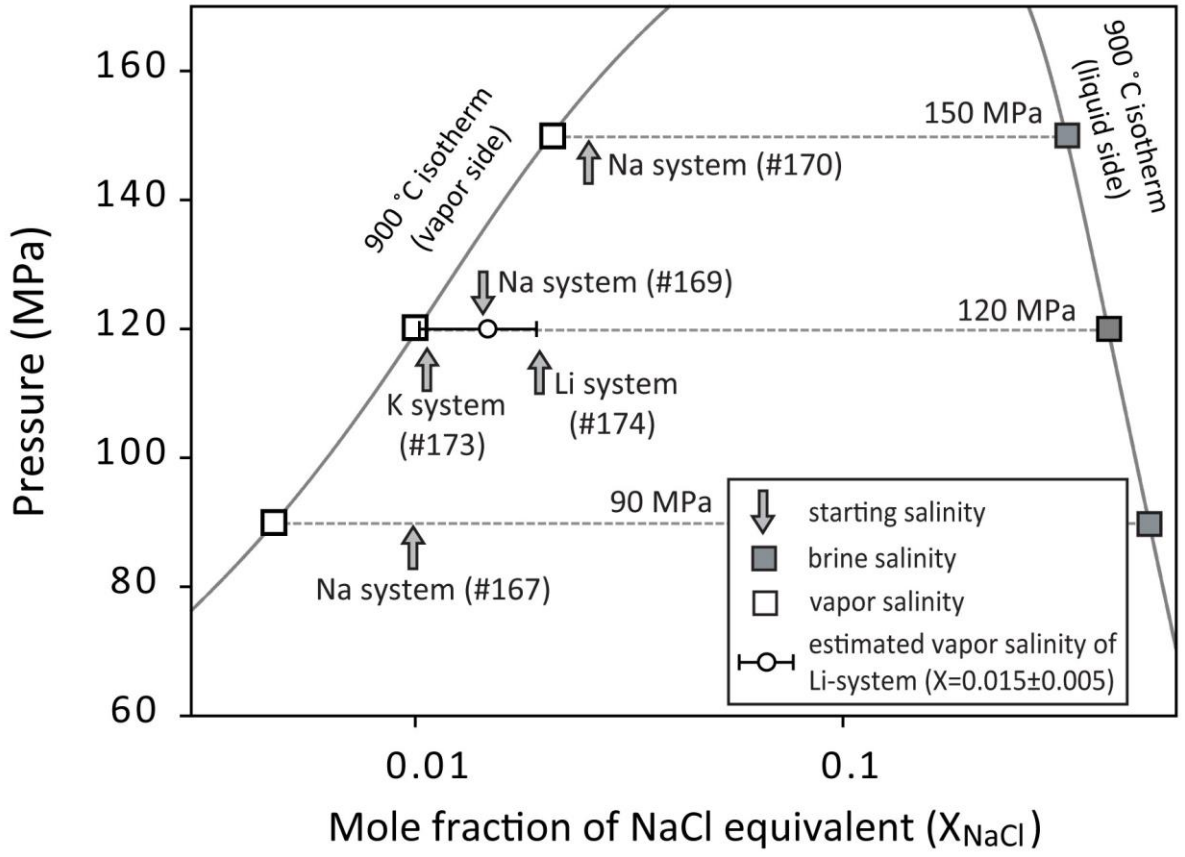

Figure 2. The phase diagram of the NaCl-H_2O system (Driesner and Heinrich, 2007) showing the solvus at 900 °C and the mole fractions of salt (X_{salt}, NaCl equivalent) in the starting solutions used in our experiments. Vapor and brine salinities in the 90, 120, and 150 MPa experiments are predicted by the algorithm of Driesner and Heinrich (2007). Salinities of the starting solutions were designed to be in between the predicted vapor and brine salinities at the respective *P-T* conditions in the H_2O-NaCl system (Driesner and Heinrich, 2007). The vapor limb of the solvus in the LiCl-H_2O system is expected to be at higher salinity relative to the NaCl-H_2O system (Dubois et al., 1994; Liebscher et al., 2007), yet brine inclusions were trapped in our experiment. Therefore, the true vapor salinity must be between that predicted for the NaCl-H2O system and the concentration in the starting solution. This yields an estimation: X_{LiCl}=0.015±0.005.

Table 2. Salinities of starting solutions and calculated values of salinity, density, and mass fraction of brine-vapor phase fluids.

	Starting solution					Model vapor				Model brine			
	Alkali	Pressure	Temp.	$X_{alkali-Cl}$	Salinity	$X_{alkali-Cl}$	Salinity[a]	Density[a]	Mass Fraction[b]	$X_{alkali-Cl}$	Salinity[a]	Density[a]	Mass Fraction[b]
		MPa	°C		wt%		wt%	g/cm^3	%		wt%	g/cm^3	%
#167	Na	150	900	0.026	7.8	0.021	6.5	0.339	97.55	0.332	61.7	0.986	2.45
#169	Na	120	900	0.014	4.5	0.010	3.2	0.257	98.02	0.416	69.8	1.071	1.98
#170	Na	90	900	0.010	3.1	0.005	1.5	0.155	97.85	0.519	77.8	1.161	2.15
#173	K	120	900	0.010	4.1	0.010[c]	4.0[d]	0.257	99.87	0.416[c]	74.7[d]	1.071	0.13
#174	Li	120	900	0.020	4.5	0.015± 0.005[e]	2.3±1.1[e]	0.257	98.18	0.416[c]	62.6[d]	1.071	1.82

[a] calculated by the NaCl-H_2O system of Driesner and Heinrich (2007)

[b] mass fraction calculated by using lever rule with the salinities of the brine, vapor, and starting solutions.

[c] mole fraction of salt ($X_{alkali-halide}$) in the K and Li system fluids equivalent to the the NaCl-H_2O system (#169 experiment) of Driesner and Heinrich (2007)

[d] recalculated salinities from the mole fractions ($X_{alkali-halide}$)

[e] estimated vapor salinity (X=0.015 and 2.3 wt%) range from mole fraction of NaCl system (0.010) to input mole fraction (0.020)

Table 3. Microthermometry (T_h and T_m salt) and calculated density (g/cm^3) of the brine inclusions in the quartz of the in-situ (IS) experiments.

	#167 (Na-halide system) 150 Mpa/ 900 °C (in-situ)			#169 (Na-halide system) 120 Mpa/ 900 °C (in-situ)			#170 (Na-halide system) 90 Mpa/ 900 °C (in-situ)			#173 (K-halide system) 120 Mpa/ 900 °C (in-situ)		#174 (Li-halide system) 120 Mpa/ 900 °C (in-situ)	
	T_m salt (° C)	T_h (°C)	Density (g/cm^3)	T_m salt (° C)	T_h (°C)	Density (g/cm^3)	T_m salt (° C)	T_h (°C)	Density (g/cm^3)	T_m salt (° C)	T_h (°C)	T_m salt (° C)	T_h (°C)
	489	949	0.95	564	1008	1.04	643	950	1.17	418	956	828	950
	494	913	0.94	571	961	1.06	643	951	1.17	427	958	831	959
	489	944	0.95	567	954	1.06	636	936	1.17	417	968	827	954
	493	990	0.95	570	949	1.06	637	1027	1.14	425	961	827	952
	492	948	0.95	570	956	1.06	662	978	1.19	426	953	828	970
	489	952	0.95	569	952	1.06	660	965	1.19	415	969	828	961
	485	941	0.94	569	955	1.06	663	989	1.19	419	978	825	958
	485	940	0.94	569	958	1.06	662	973	1.19	420	963	826	972
	488	946	0.94	580	896	1.09	668	969	1.20	414	1039	827	979
	490	952	0.95	565	957	1.05	662	999	1.18	426	981	830	971
AV	489	947	0.95	569	955	1.06	653	974	1.18	420	973	827	963
STD	3	19	0.00	4	27	0.01	12	27	0.02	5	25	2	10

footnote: AV and STD represent average temperatures and standard deviation (1 σ), respectively.

2.2. *Analytical methods*

Singly-targeted brine inclusions were analyzed with an ICP-Quadrupole-MS (Perkin Elmer Elan 6100 DRC) connected to the ETH-prototype 193 nm ArF excimer laser (GeoLas laser ablation system; (Günther et al., 1997) at ETH Zurich. We used a laser energy density between 30 and 40 J/cm^2 and repetition rates of 10 Hz and an iris aperture to open the quartz host gradually from 10 µm up to a crater size larger than the targeted fluid inclusion. We used an in-house built aluminum ablation cell with small internal volume (1cm^3). ICP gas backgrounds and sensitivities were optimized for the detection of Cl and Br (Seo et al., 2011). We added a small amount of H_2 gas (5 ml/min) into the He carrier stream (Guillong and Heinrich, 2007) and used increased dwell times of 50 ms on ^{35}Cl and 100 ms on ^{79}Br (10 ms on ^{7}Li, ^{23}Na, and ^{39}K) to reduce the noises of the gas backgrounds for optimal limits of detection for Cl and Br (Fig. 1B). Since we could not obtain statistically significant Cl and Br signals due to their low-density and smaller size, direct analysis of the Cl/Br ratios in the vapor inclusions was not possible. Absolute vapor salinities, and therefore vapor/brine mass fractions could not be calculated from the analysis of vapor inclusions either, because we did not have an independent internal standard to quantify absolute element concentrations.

As an external standard, a previously characterized natural scapolite (Sca17) was used for Li, Na, K, Cl and Br (Guillong et al., 2008; Seo et al., 2011). Element ratios obtained by LA-ICP-MS were converted into absolute concentrations (Heinrich et al., 2003) using Cl as an internal standard, concentrations of which were obtained from the calculated brine salinities estimated for the NaCl-H_2O system for the applied *P-T* conditions (Driesner and Heinrich, 2007). The Cl concentrations in the brine inclusions in the K and Li-bearing systems were obtained by the same method. We used Cl as an internal standard because Cl is the only common major element in every alkali halideH_2O experiments. Unfortunately, the measured salt melting temperatures in the K and Li-rich systems by a microthermometry (Table 3) could not be converted to the salt concentrations in the absence of appropriate experimental data for the applied *P-T* conditions. Using analogy to the NaCl-H_2O system introduces some uncertainties in the calculated absolute element concentrations; however, it does not affect the analyzed element ratios in brine inclusions. Note that the element ratios themselves are independent of the choice of internal standards for the quantification of absolute concentrations. Errors of each analysis were calculated as 1 standard deviation of the concentrations and Cl/Br mass ratios of all single-inclusion analyses in one experimental run (numbers of analyzed inclusions in an assemblage = 6-9, Table 4).

To examine the possible isobaric interference of ^{79}KAr on ^{79}Br, we investigated LA-ICP-MS transient signals obtained from analysis of separately prepared K-rich and Br-absent synthetic brine inclusions (Fig. 3A). No apparent Br signal was observed in this analysis and the calculated count ratio of KAr/K was lower than 0.001%. Moreover, transient signals obtained from natural brine inclusion (free-standing quartz crystal in miarolitic cavity of Chernomoretz intrusions, Bulgaria) shows different maximum positions of ^{79}Br and ^{39}K signals, due to the presence of a Br-rich solution and a KCl daughter crystal ablated somewhat later (Fig. 3B). The evidence from synthetic and natural fluid inclusion analyses shows that the ^{79}KAr isobaric interference on ^{79}Br analysis is negligible. Previous analyses of synthetic liquid inclusions of variable Cl/Br ratios demonstrated good accuracy and a typical range of uncertainties of 7-24% (1σ relative; Seo et al.,

2011).

Table 4. Compositions of analyzed brine inclusions with Cl internal standardization where Cl concentrations were obtained from calculated brine salinities. The com position of vapor inclusions were calculated by mass balance using the analyzed brine compositions, the known composition of the starting solution and calculated mass fractions of vapor and brine. IS and PF refer to in-situ fractured and pre-fractured, respectively.

				Brine composition (LA-ICP-MS: Cl internal standard)							Calculated vapor composition					
	Info	size µm	X_{salt} brine	Li µg/g	Na µg/g	Cl µg/g	K µg/g	Br µg/g	Cl/Br mass ratio	X_{salt} vapor	Li µg/g	Na µg/g	Cl µg/g	K µg/g	Br µg/g	Cl/Br mass ratio
#167 (Na-halide aqueous system) 150 Mpa/ 900 °C, input Cl/Br ppm ratio = 7.6																
11mr09c07	IS	20			250'000			41'000	9.2			24'000			4'800	7.3
11mr09c08	IS	30			260'000			37'000	10.1			24'000			4'900	7.1
11mr09c09	IS	25			240'000			37'000	10.2			24'000			4'900	7.1
11mr09c11	IS	15			280'000			34'000	11.0			23'000			5'000	7.0
11mr09c12	IS	20			270'000			34'000	11.0			24'000			5'000	7.0
11mr09c14	PF	30			230'000			34'000	11.0			25'000			5'000	7.0
11mr09c16	IS	25			240'000			31'000	12.0			24'000			5'000	6.9
AV			***0.332***		***250'000***	***370'000***		***35'000***	***10.6***	***0.021***		***24'000***	***35'000***		***4'900***	***7.1***
STD (1σ)					***16'000***			***3'100***	***0.9***			***400***			***77***	***0.1***
#169 (Na-halide aqueous system) 120 Mpa/ 900 °C , input Cl/Br ppm ratio = 7.8																
14oc14b05	IS	30			340'000			34'000	12.5			10'500			2'600	6.6
14oc14b06	IS	20			280'000			37'000	11.3			11'700			2'500	6.7
14oc14b10	IS	30			380'000			41'000	10.4			9'800			2'400	6.9
14oc14b12	IS	20			310'000			40'000	10.6			11'300			2'500	6.9
14oc14b15	IS	20			320'000			44'000	9.7			11'000			2'400	7.1
14oc14b18	IS	30			330'000			44'000	9.6			10'900			2'400	7.1

14oc14b25	IS	30		340'000		41'000	10.3		10'500			2'400	6.9
14oc14b28	IS	30		290'000		44'000	9.6		11'500			2'400	7.1
14oc14b30	IS	20		320'000		42'000	10.1		11'000			2'400	7.0
AV			***0.416***	***320'000***	***420'000***	***41'000***	***10.5***	***0.010***	***10'900***	***16'900***		***2'400***	***6.9***
STD (1σ)				***28'000***		***3'400***	***0.9***		***570***			***68***	***0.2***
#170 (Na-halide aqueous system) 90 Mpa/ 900 °C, input Cl/Br ppm ratio = 7.8													
11mr09d09	IS	25		320'000		50'000	9.4		5'100			1'170	6.3
11mr09d10	IS	30		310'000		45'000	10.4		5'300			1'280	5.8
11mr09d11	IS	25		330'000		48'000	9.8		4'800			1'220	6.0
11mr09d12	IS	35		330'000		41'000	11.6		4'900			1'380	5.3
11mr09d14	IS	30		340'000		45'000	10.5		4'600			1'290	5.7
11mr09d15	IS	20		340'000		40'000	11.7		4'700			1'380	5.3
AV			***0.519***	***330'000***	***470'000***	***45'000***	***10.6***	***0.005***	***4'900***	***7'300***		***1'280***	***5.7***
STD (1σ)				***11'900***		***3'900***	***0.9***		***260***			***86***	***0.4***
#173 (K-halide aqueous system) 120 Mpa/ 900 °C, input Cl/Br ppm ratio = 8.5													
11mr10a06	IS	25			450'000	43'000	8.3				21'000	2'100	8.5
11mr10a07	IS	20			480'000	36'000	9.9				20'000	2'100	8.4
11mr10a08	IS	25			450'000	35'000	10.3				21'000	2'100	8.4
11mr10a09	IS	30			420'000	41'000	8.6				21'000	2'100	8.5
11mr10a10	IS	25			500'000	43'000	8.3				20'000	2'100	8.5
11mr10a12	IS	35			470'000	41'000	8.6				21'000	2'100	8.5
11mr10a14	PF	30			480'000	33'000	10.6				20'000	2'100	8.4

11mr10a15	PF	20				500'000	34'000	10.5				20'000	2'100	8.4
11mr10a17	PF	20				500'000	34'000	10.3				20'000	2'100	8.4
AV			***0.416***		***360'000***	***470'000***	***38'000***	***9.5***	***0.010***		***17'700***	***21'000***	***2'100***	***8.4***
STD (1σ)						***28'000***	***4'200***	***1.0***				***37***	***6***	***0.0***
#174 (Li-halide aqueous system) 120 Mpa/ 900 °C, input Cl/Br ppm ratio = 8.1														
11mr10c05	IS	25		161'000			36'000	14.4		4'100			3'600	6.9
11mr10c07	IS	25		177'000			35'000	14.8		3'800			3'600	6.8
11mr10c11	IS	20		170'000			28'000	18.7		4'000			3'700	6.6
11mr10c12	IS	30		163'000			33'000	15.8		4'100			3'700	6.8
11mr10c13	IS	25		171'000			30'000	17.3		3'900			3'700	6.7
11mr10c15	PF	30		160'000			27'000	19.3		4'100			3'800	6.6
11mr10c16	PF	35		164'000			28'000	19.0		4'100			3'800	6.6
11mr10c17	PF	50		153'000			35'000	14.8		4'300			3'600	6.8
11mr10c18	PF	40		161'000			36'000	14.7		4'100			3'600	6.8
AV			***0.416***	***164'000***	***520'000***		***32'000***	***16.5***	***0.015***	***4'100***	***25'000***		***3'700***	***6.7***
STD (1σ)				***7'100***			***3'800***	***2.0***		***132***			***71***	***0.1***
					vapor composition in Li-system calculated with mole fraction in vapor of 0.020 →				***0.020***	***6'900***	***34'000***		***4'200***	***8.0***
										2			***1***	***0.0***
					vapor composition in Li-system calculated with mole fraction in vapor of 0.010 →				***0.010***	***1'160***	***15'700***		***3'200***	***5.0***
										260			***140***	***0.2***

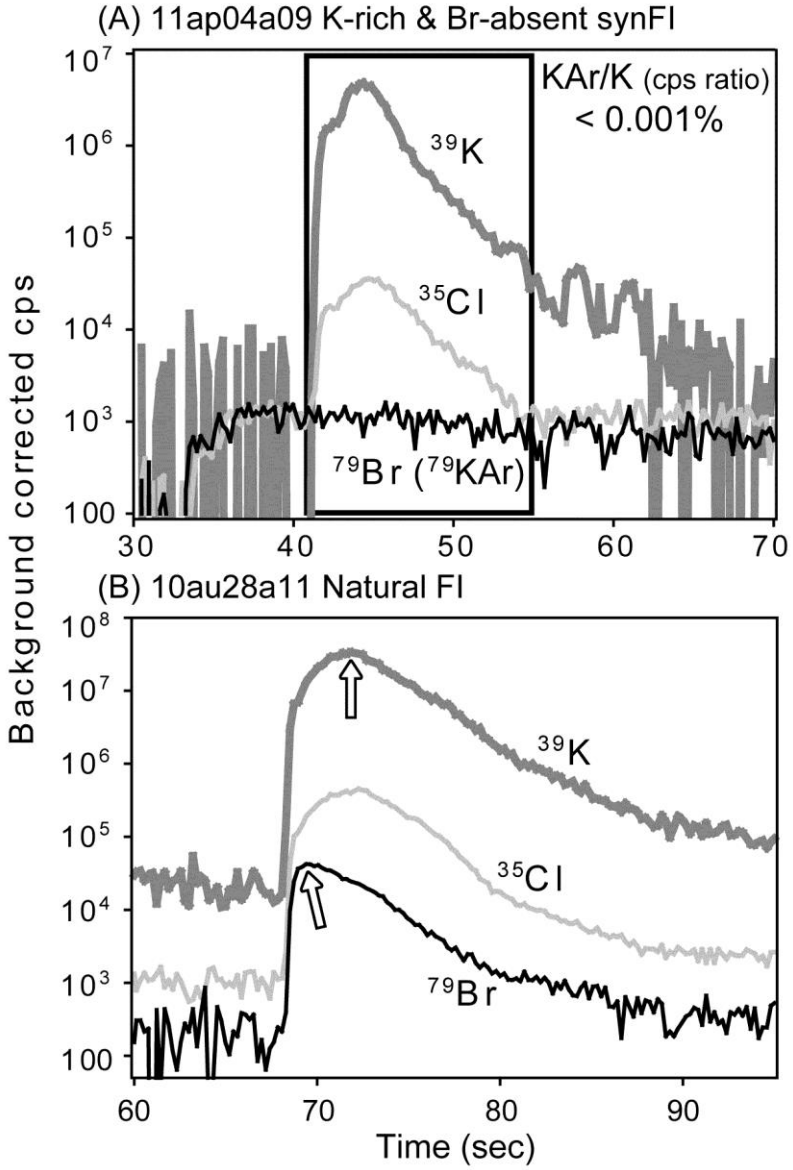

Figure 3. LA-ICP-MS transient signals of (A) synthetic K-rich and Br-absent brine inclusions, and (B) natural brine inclusion to check ^{79}KAr polyatomic interference on ^{79}Br analysis. **(A)** Synthetic inclusion analysis showing less than 0.001% of KAr/K cps ratio; and **(B)** natural inclusion showing different times of maximum peaks of ^{39}K and ^{79}Br indicating that the argide formation is not significant for KAr interference on Br.

2.3. Calculations of fluid density, salinity, and vapor composition

The densities and salinities of entrapped brine and vapor phases in each experiment were calculated using the model of Driesner and Heinrich (2007) for the NaCl-H_2O model system (Table 2). Since halogen ratios in the vapors could not be directly derived from LA-ICPMS analyses, we calculated the Cl/Br ratio in the vapors by mass balance by using the analyzed compositions of brine inclusions, the known composition of the starting solutions and the estimated vapor/brine mass fractions (Driesner and Heinrich, 2007). The same method was applied for the K- and Li-bearing systems, assuming KCl + KBr in K-system and LiCl + LiBr in Li-system are equivalent to NaCl, since there is only a few experimental data available for K and Li halides aqueous systems (Heinrich, 2007; Liebscher, 2007). An error could arise from the above assumption when

calculating brine-vapor mass fractions, the extent of which was estimated. The vapor salinities and critical points in the KCl-H_2O system (Hovey et al., 1990; Dubois et al., 1994; Shmulovich et al., 1995) are comparable to those in the NaCl-H_2O system (Driesner and Heinrich, 2007), and the position of the two phase curves are nearly identical (Hovey et al., 1990). Therefore, we applied vapor salinities for the K halide – H_2O system equal to those predicted for the NaCl-H_2O system (X_{salt}=0.010, Table 2, Driesner and Heinrich, 2007). It is important to note the all above data are for temperatures below 600 °C. The salinities on the vapor limb of the solvus in the LiCl-H_2O system are higher compared to the NaCl-H_2O system (Dubois et al., 1994; Liebscher et al., 2007) at a given *P-T*. Therefore, by using vapor salinities for the NaCl-H_2O model system, we would likely overestimate the mass fraction of brine in the Li halide-bearing experiment (Liebscher et al., 2007). Therefore, we estimated the possible error on the such-derived vapor salinities in the Li halide – H_2O system. Since we have trapped both brine and vapor inclusions (Fig. 1), our starting fluid (salinity of X_{salt}=0.020 or 4.5 wt%) must have entered the two phase field. Therefore, it is safe to assume that the salinity of the vapor in the Li-system are higher than that estimated by analogy to the NaCl-H_2O system (X_{salt}=0.010), but lower than the salinity of the starting solution ($X_{Li\text{-}halide}$=0.020). We thus assumed a vapor salinity of $X_{Li\text{-}halide}$=0.015±0.005 (Table 2) and discuss the resulting propagated error on the Cl/Br ratios in the following chapters.

Mass fractions of brine and vapor phases were calculated from the starting salinities by applying "lever rule" on the NaCl-H_2O model system for the apparent *P-T* (equation 1). The vapor compositions were calculated by a mass balance using the analyzed brine compositions according to the equation 2 (Table 2 and 4).

$$\text{Salinity}_{\text{starting}} = X_{\text{vapor}} * \text{Salinity}_{\text{vapor}} + X_{\text{brine}} * \text{Salinity}_{\text{brine}} \quad (1)$$

$$\text{Concentration}_{\text{starting}} = X_{\text{vapor}} * \text{Concentration}_{\text{vapor}} + X_{\text{brine}} * \text{Concentration}_{\text{brine}} \quad (2)$$

In the equation 1, $\text{Salinity}_{\text{vapor}}$ and $\text{Salinity}_{\text{brine}}$ were calculated using equivalent concentrations from the NaCl-H_2O system (Driesner and Heinrich, 2007), and refer to the wt% of the sum of total alkali halides in starting solution, vapor, and brine, respectively. X_{vapor} and X_{brine} refer to the mass fraction of vapor and brine relative to the starting fluid.

3. RESULTS

Microthermometry of the brine inclusions in the in-situ (IS) experiments showed consistent homogenization and the salt melting temperatures in each experiment (Table 3). The homogenization temperatures (T_h) fell within narrow ranges from 947±19 °C to 974±25 °C, confirming that the brine inclusions were free of vapor contamination. The somewhat higher T_h relative to the trapping temperature (900 °C) is likely due to the stretching of the host quartz during the reheating experiment. It could also be due to the co-entrapment of a minor amount of vapor phase though the consistent homogenization temperatures are against this assumption. Nevertheless, even if the higher Th is due to vapor contamination, the addition of such minor amount of vapor would cause very little bias on the brine compositions. Brine salt melting temperatures of the Li halide system (827±2 °C, #174) were higher compared to Na halide (569±4 °C, #169) and K halide – H_2O (420±5 °C, #173) system from the 120 MPa / 900 °C experiments.

We report the analyzed Cl/Br ratios in brine inclusions in the pre-fractured (PF) and in the in-situ fractured (IS) quartz (Table 4). The Cl/Br ratios are higher in analyzed brines compared to the starting solutions to variable degrees (Fig. 4 and Table 4). In the Na halide – H_2O, the analyzed Cl/Br ratio in the brine inclusions from experiment #167 (150 MPa/900 °C) is 10.6±0.9 whereas the starting Cl/Br ratio is 7.6, the Cl/Br ratio in the brine from experiment #169 (120 MPa/900 °C) is 10.5±0.9 whereas the starting ratio is 7.8, and the same quantity for experiment #170 (90 MPa/900 °C) is 10.6±0.9 while the starting ratio is 7.8 (Table 4). In the K halide – H_2O system, the analyzed Cl/Br ratios in the brine from experiment #173 (120 MPa/900 °C) is 9.5 ± 1.0 whereas the starting Cl/Br ratio is 8.5 (Table 4). In the Li halide – H_2O system, the analyzed Cl/Br ratio in the brine (#174, 120 MPa/900 °C) is 16.5±2.0 whereas the starting Cl/Br ratio is 8.1. Chlorine is relatively enriched compared to Br in the brine phase fluids compared to the starting solutions and therefore even more relative to the vapor phase, with the greatest preferential partitioning in the Li halide – H_2O system and less pronounced but still significant effects in the K and Na halide dominated systems (Fig. 4).

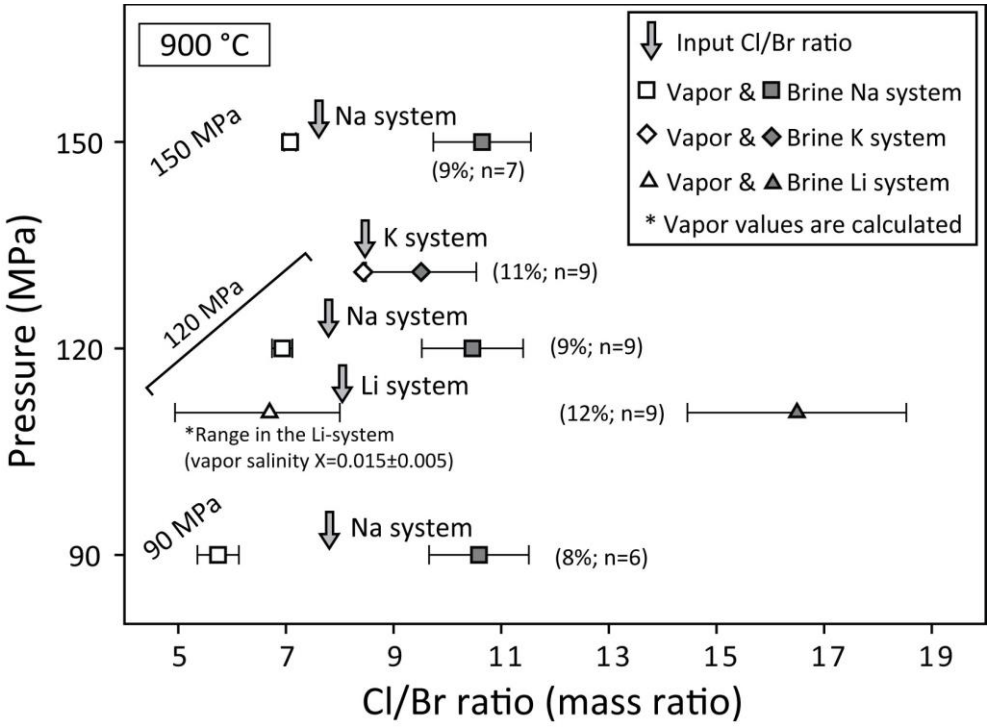

Figure 4. Cl/Br ratios as measured in the brine inclusions, known for the starting solutions, and calculated for the vapor inclusions. Errors in the brackets represent % of 1σ/average of the brine inclusions in each experimental runs, the errors on the calculated vapor compositions in the Li halide – H_2O system contain the uncertainty on the estimation of vapor/brine mass ratios as well as the analytical error on brine inclusion analysis. For the Na and K-halide system, the errors are calculated only from the brine inclusion analysis

The Cl/Br ratios in the vapors are calculated by using the equations 1 and 2. In the Na halide – H_2O system, the calculated Cl/Br ratio in the vapor of #167 run (150 MPa/900 °C, vapor salinity X=0.021) is 7.1±0.1, the vapor of #169 run (120 MPa/900 °C, vapor salinity X=0.010) is 6.9±0.2, and the vapor of #170 (90 MPa/900 °C, vapor salinity X=0.005) is 5.7±0.4 (Table 4). In the K halide – H_2O system, the calculated Cl/Br ratios in the vapor of #173 run (120 MPa/900 °C) with vapor salinity of X=0.010 is 8.4±0.0 (Table 4). The vapor of Li halide – H_2O system (#174 run, 120

MPa/900 °C) has salinity range of X=0.015±0.005, and calculated Cl/Br ratios are 5.0±0.2 when X=0.010, 6.7±0.1 when X=0.015, and 8.0±0.0 when X=0.020. Therefore, the Cl/Br ratio in the Li halide-bearing vapors is constrained to be between 4.8 and 8.0 (Table 4 and Fig. 4).

Mass-based density ratios of vapor/brine are 0.34, 0.24, and 0.13 in the 150, 120, and 90 MPa experiments, respectively (Table 2). It appears, however, that the density contrast in this range does not yield a statistically significant difference in the degree of Cl/Br fractionation (Fig. 4).

We compared the total charge balances of alkali metals and halogens (Cl+Br) in the analyzed brines (Fig. 5). The molar alkali/halogen ratios are 1.15±0.07, 1.13±0.10, and 1.56±0.07 in the brines of the K halide – H_2O, Na halide – H_2O and Li halide – H_2O systems, respectively, indicating an apparent excess of alkalis over halogens with the greatest imbalance in the Li halide – H_2O system.

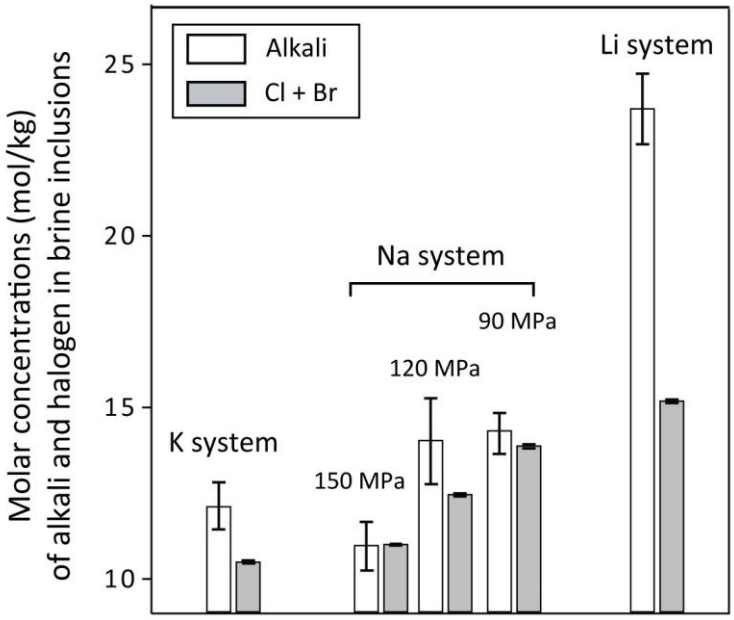

Figure 5. Molar balances of alkali ions (mol/kg of K or Na or Li) and halide ions (mol/kg of Cl + Br) in the analyzed brine inclusions showing excess of alkali metals relative to halogens. Li halide – H_2O system has highest discrepancy of alkali and halogen concentrations compared to the K and Na halide – H_2O systems. Error bars represent 1σ on the concentrations in brines for each experimental run.

Fractionation of Cl/Br between vapor and brine is compared as a function of density contrasts (Fig. 6A) and the identity of alkali metals in the system (Fig. 6B). The exchange coefficient of Cl/Br ratios between vapor and brine ($K_{Cl/Br}^{vapor/brine}$) in the 150, 120, and 90 MPa experiments are 0.7±0.1, 0.7±0.1, and 0.5±0.1, respectively (Fig. 7 and Table 4). It appears that the density contrast does not have a statistically significant effect on $K_{Cl/Br}^{vapor/brine}$ apart from a minor difference between the 90 and 120 MPa experiments (Fig. 7). Partitioning of Br and Cl is dependent on the identity of alkali metals in the system (Fig. 6B), and $K_{Cl/Br}^{vapor/brine}$ is strongly dependent on the identity of the alkali metals (Fig. 7). The values of $K_{Cl/Br}^{vapor/brine}$ in the Na and K halide – H_2O system at 120 MPa and 900 °C are respectively 0.7±0.1 and 0.9±0.1, whereas in the Li halide – H_2O system, the same

quantity is 0.4±0.2 (Fig. 7 and Table 4). It is apparent that the Li halide – H_2O system exhibits by far the greatest Cl/Br fractionation between vapor and brine (Fig. 6 and 7).

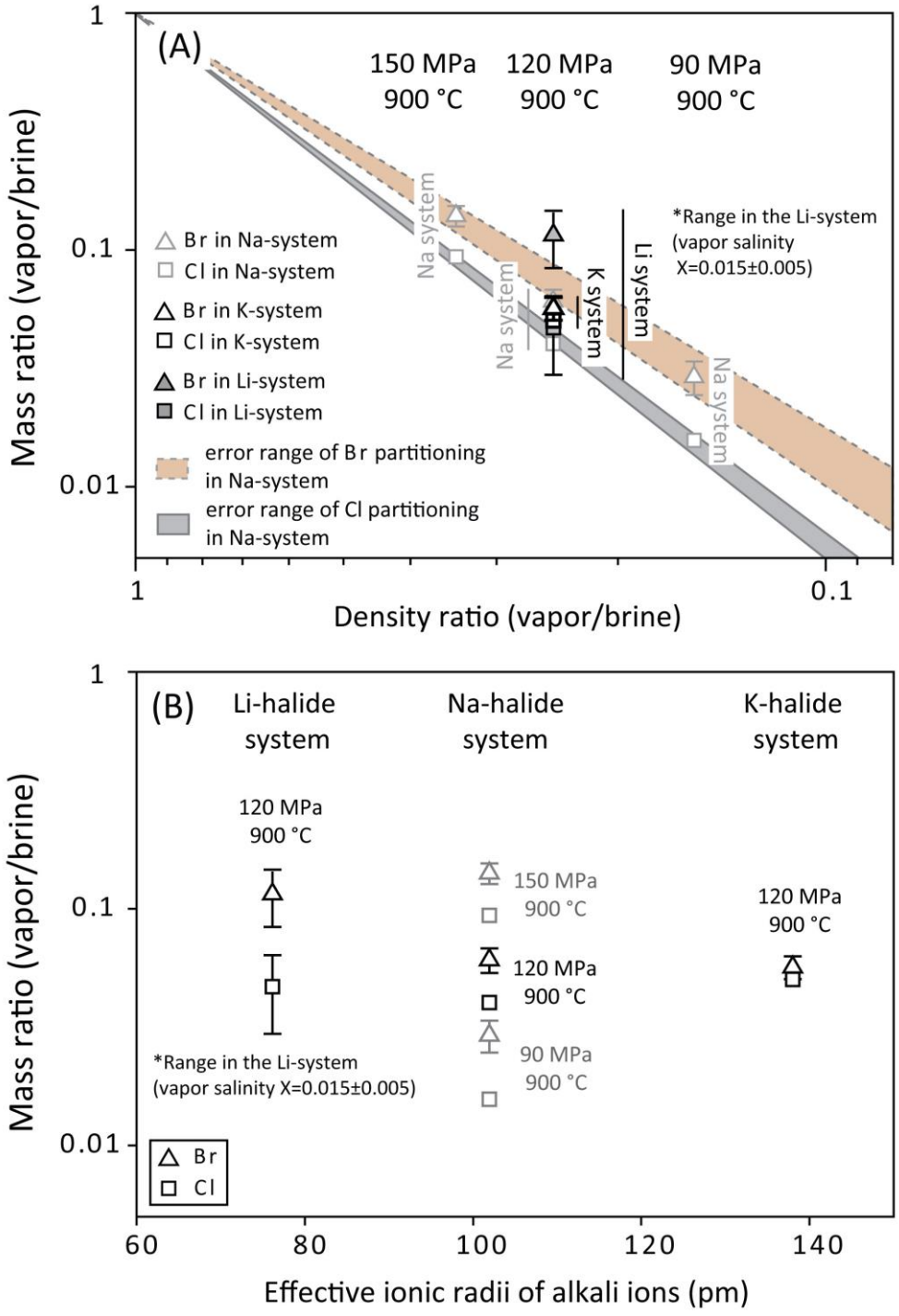

Figure 6. Plots of Cl_{vapor}/Cl_{brine} and Br_{vapor}/Br_{brine} mass ratios for various alkali-halide – H_2O systems vs. (**A**) vapor/brine density ratios and (**B**) effective ionic radii of alkali ions. The partitioning of Br and Cl is dependent on the ratio of vapor and brine densities. Bromine partitions strongly into the vapor in the Li halide – H_2O system compared to other alkali systems. The degree of halogen element fractionation in the K halide – H_2O system is the smallest. The brackets of Li-system represent the estimated possible error range with vapor salinity of X_{salt}=0.015±0.005, while errors in the other brackets represent % of 1σ/average.

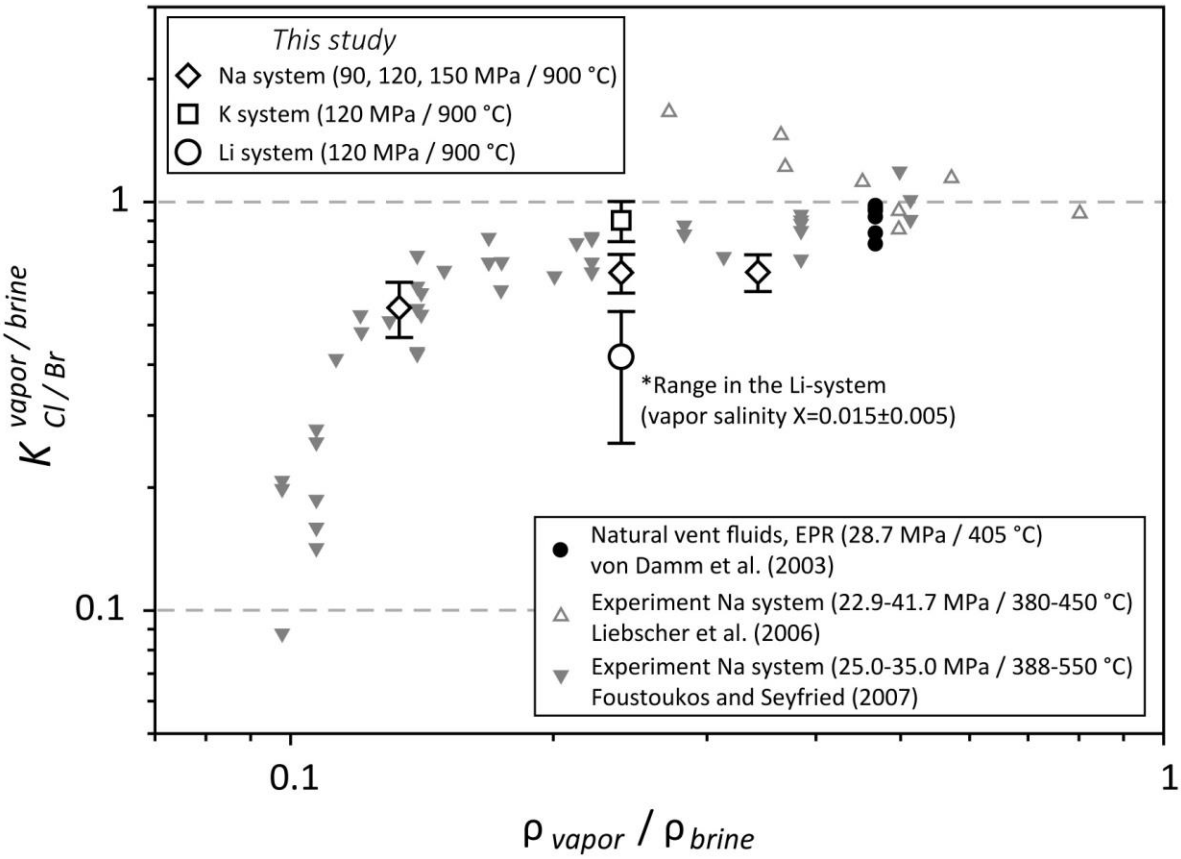

Figure 7. Ratios of Cl/Br_{vapor} and Cl/Br_{brine} ($K^{vapor/brine}_{Cl/Br}$) as a function of vapor/brine density contrast. Natural vent fluid sampled from the East Pacific Rise and other previous experimental results from the literature (Von Damm et al., 2003; Liebscher et al., 2006; Foustoukos and Seyfried, 2007) were plotted for comparison. The brackets of Li-system represent the estimated range with vapor salinity of X_{salt}=0.015±0.005, while errors in the other brackets represent % of 1σ/average of $K^{vapor/brine}_{Cl/Br}$.

4. DISCUSSIONS and GEOLOGICAL IMPLICATIONS

We now discuss a mechanism of Br/Cl fractionation during vapor-liquid immiscibility and suggest some geological implications of this phenomenon in magmatic-hydrothermal systems.

4.1. Alkali-halogen molar imbalance in the brine phase

The fractionation of Br and Cl between vapor and brine phase (Fig. 4 and 6) can be explained by comparing the stability of competing alkali-halide and alkali-OH ion pairs in high-temperature aqueous fluids. Conductivity measurements of electrolyte-bearing aqueous solution showed that the degree of ion association greatly increases at high temperatures (Ho et al., 2000a). Electrolytes such as alkali-halide and alkali-OH have particularly high association constant (K_A) in low-density dilute aqueous solutions at high temperature, i.e. in vapor-like fluids (Ho et al., 1994; Ho and Palmer, 1996, 1997, 1998; Ho et al., 2000b). We suggest that differences in the stability of alkali-Cl, alkali-Br and alkali-OH ion pairs at the high-temperatures (Fournier, 1987; Shmulovich et al., 1995; Bischoff et al., 1996) applied in the current experiments are responsible for the fractionation of Cl/Br between brine and vapor. This can be expressed by the following exchange reaction among $alkali^+$ — H^+ (cations), and $halide^-$ — OH^- (anions or ligands):

$$\text{alkali-halide} + H_2O \rightarrow \text{alkali-OH}_{\text{liquid (brine)}} + \text{H-halide}_{\text{vapor}} \quad (3)$$

Relatively higher stability of alkali-OH ion pairs compared to alkali-chlorides at temperatures higher than 400 °C will shift the reaction to the right (Ho et al., 1994; Ho and Palmer, 1996, 1997, 1998; Ho et al., 2000b). The H-halides such as HCl and HBr are known experimentally to be partitioned into the vapor phase fluid (Williams et al., 1997; Palmer et al., 2004), whereas alkali-halide and alkali-OH prefer more hydrated environments such as the brine phase (Fournier and Thompson, 1993; Williams-Jones et al., 2002; Palmer et al., 2004). The observed excess of alkali metals over halogens in the brines (Fig. 5) indicates the presence of alkali-OH in the brines according to equation 3.

The relatively higher halogen concentrations in the vapor phase in the Li halide – H_2O system compared to K and Na halide – H_2O system (Fig. 6) might be explained by different association degrees of LiOH, NaOH, and KOH affecting the efficiencies of H-halide production. Association constants of LiOH, NaOH, and KOH in high-temperature (above 400 °C) dilute aqueous solutions have been estimated by conductivity measurements (Ho and Palmer, 1996, 1997, 1998). The association constant (K_A) are in the order of LiOH > NaOH ≥ KOH, and the calculated K_A are respectively 6485, 3809, 2040 in 600 °C and 0.4 g/cm^3 solutions (Ho et al., 2000b). The stronger association of LiOH compared to NaOH and KOH would lead to the formation of more HBr and HCl in the Li halide – H_2O system, which in turn would preferentially partition into the vapor (Fig. 6). This argument is consistent with the larger molar imbalance between Li and halogens analyzed in the brine phase of the Li-system relative to that observed in the K- and Na-system (Fig. 5).

4.2. Preferential Br partitioning into the vapor phase fluids

The relatively stronger vapor partitioning of Br compared to Cl can be interpreted by the association degrees of alkali-Cl and alkali-Br. Conductivity measurement of NaCl and NaBr aqueous solutions at 330-400 °C showed higher association constant of NaCl compared to NaBr (Gruszkiewicz and Wood, 1997). While experimental studies for LiBr and KBr are lacking, we assume that the other alkali chlorides (K and Li) are also more strongly associated than the alkali bromides because of the higher electron negativity of Cl compared to that of Br. Higher association constant of NaCl compared to NaBr will lead to a lower equilibrium constant for equation 3, thus less HCl will form compared to HBr, which in turn would result in the observed preferential Br partitioning into the vapor phase fluids relative to Cl (Fig. 6). This may be further enhanced by variability in the stability of H-halides. These are covalently bonded molecules and such bonds tend to be stronger when the difference in the electronegativity of constituent atoms are smaller (Jolly, 1984). The difference of electronegativity for HBr is 0.7, whereas for HCl it is 0.9, therefore HBr is likely a more stable species. It is important to note, that quartz would react with alkali-hydroxide species formed during reaction 1 to produce various alkali-silicate species (Anderson and Burnham, 1967). This would, however, likely not affect the above described systematics to a significant extent as these would also likely partition into the brine phase.

Since we assume that alkali-OH may be a significant species in the brines, especially in the Li – halide bearing system, we must consider the uncertainty this causes on the estimation of vapor salinities. We know of experimental data only in the NaOH-H_2O system (Urusova, 1974), which was compared to the NaCl-H_2O system (Liebscher, 2007). While the critical curves are similar, the

vapor limb of the solvus of the NaOH-H_2O system at 350 - 550 °C is shifted towards somewhat higher salt concentrations compared to that in the NaCl-H_2O system (Driesner and Heinrich, 2007). Therefore, the presence of alkali-OH and H-halides would likely increase the vapor salinity and this would be most pronounced in the Li halide-bearing system. Yet we have trapped brine inclusions in this experiments, which limits the possible vapor salinity in between the value model calculated for the NaCl-H_2O system and the salinity of the starting solution used for the experiment. We have previously accounted for this uncertainty and it was propagated into the error bars on all figures.

4.3. Comparison to previous studies

Previous hydrothermal experiments yielded contradictory results. Liebscher et al. (2006) determined that Cl preferentially partitions into the vapor phase relative to Br at vapor/brine density ratios of 0.27-0.80 and T=380–450 °C, whereas Foustoukos and Seyfried (2007) reported preferential Br partitioning into the vapor phase at vapor/brine density ratios of 0.10-0.51 and T=388–550 °C (Fig. 7). Our experiments conducted at 900 °C within a narrower range of the vapor/brine density ratios of 0.13 - 0.34 yielded results that are consistent with those of Foustoukos and Seyfried (2007), showing lower Cl/Br ratios in the vapors than in the brines. Natural hydrothermal fluids with the vapor/brine density ratios of 0.47 at 405 °C sampled from a sub-seafloor hydrothermal vent in the East Pacific Rise also show preferential Br partitioning into the vapor phase (Von Damm et al., 2003). The geochemical cause for the discrepancy with the data of Liebscher et al. (2006) is unclear. Experiments of Foustoukos and Seyfried (2007) were conducted at somewhat higher temperature up to 550 °C and showed lower pH in the coexisting vapor phase, which might indicate the formation of alkali-OH and H-halides in high-temperature fluids consistent with our interpretation. Both the studies of Liebscher et al. (2006) and Foustoukos and Seyfried (2007) identified that the vapor/brine density contrast affects the extent of Cl/Br fractionation during phase separation (Fig. 7). We also found the density contrast effect on Cl/Br fractionation in the high-temperature (900 °C) Na halide – H_2O system between the 90 MPa experiment and the 120 MPa experiments, while the effect is not apparent between the 120 and 150 MPa experiments within the analytical error (9-10 %). This might be because the 120 and 150 MPa experiments are closer to the critical point of the Na halide – H_2O system (Fig. 2). Although we could not observe a significant density contrast effects, the precision of our analysis was sufficient to observe large differences in the degree of Cl/Br fractionations produced by the alkali ions in solution (Fig. 4 and 7). Also, it should be noted that the density range in our experiments is relatively small in comparison to those in the lower-*T* studies (Fig. 7). Density range in our experiments are 0.15-0.34 g/cm^3 in vapors and 0.99-1.16 g/cm^3 in brines, while studies of Liebscher et al. (2006) and Foustoukos and Seyfried (2007) have the vapor densities of 0.11-0.46 g/cm^3 and the liquid densities of 0.57-1.18 g/cm^3.

4.4. Geological implications

The *P-T* conditions of this study are applicable to magma degassing and the magmatic-hydrothermal transition. A major implication of our study is that the Cl/Br fractionation between the immiscible vapor and brine will be significantly influenced by the types of alkalis present in the high-temperature hydrothermal system. Although the dissolved salt components in the natural high-temperature aqueous fluids are dominated by NaCl, KCl and $FeCl_2$, and $CaCl_2$ at some

conditions, preferential Br partitioning into the vapors could be very significant in Li-rich hydrothermal systems such as those forming Li-pegmatites or when the fluid experiences extreme phase separation near to the vapor-liquid-halite field (Foustoukos and Seyfried, 2007; Klemm et al., 2007). Caution is required when inferring the source of halogens in magmatic-hydrothermal fluids from Cl/Br ratios in natural fluid inclusions (Gleeson and Smith, 2009; Nahnybida et al., 2009) as determined by bulk crush-leach methods (Bray and Spooner, 1992). Brine phase fluids have relatively high densities with high Si content, which might lead to wetting properties superior to those of the vapor when they come in physical contact with silicate minerals (Roedder, 1984; Sterner and Bodnar, 1984) . Therefore, brine inclusions are more likely to be entrapped in silicate minerals compared to the low-density vapor-like fluids and the average trapped fluid composition may not be truly representative of the Cl/Br ratio of the original hydrothermal fluid, even if only a single generation of inclusions was trapped in the host mineral.

5. CONCLUSIONS

Our experiments showed that the vapor phase is characterized by higher Br/Cl ratios relative to the brine in various alkali halide – H_2O systems. The degree of the Cl/Br fractionation is highly affected by the identity of the alkali metal present in the solution. The observed relatively high degree of Cl/Br fractionation in the Li halide – H_2O system and lower degrees of Cl/Br fractionations in K and Na halide – H_2O systems might be attributed to the formation of associated alkali-OH and hydrogen-halide species in the high-temperature fluids. The argument is supported by the measured alkali excess over halogens in our brine inclusions and the low pH in the coexisting vapors as reported by Foustoukos and Seyfried (2007). Nevertheless, our study indicates that not much Cl/Br fractionation would happen during fluid phase separation in normal Na-K-dominated geological fluids at magmatic temperatures except for extremely Li-rich systems.

ACKNOWLEDGMENTS

We thank Marcel Guillong for a discussion about K-argide interference in ICP-MS, Thomas Driesner for a discussion about high-temperature hydrothermal geochemistry, and Christoph Heinrich for many valuable suggestions and discussions. We appreciate the constructive reviews of Axel Liebscher, Jim Webster and Dionysis Foustoukos, and many additional helpful comments from Associate Editor, Gleb Pokrovski. J. H. Seo acknowledges the support of the project PE15050 funded by the Korea Polar Research Institute (KOPRI) and the Inha University Research Grant (INHA-48580). Z. Zajacz acknowledges the support of the Swiss National Science Foundation (project no. PZ00P2_136857) and the Discovery Grant program of the Natural Sciences and Engineering Research Council of Canada.

REFERENCES

Anderson, G.M., Burnham, C.W., 1967. Reaction of quartz and corundum with aqueous chloride and hydroxide solutions at high temperatures and pressures. American Journal of Science 285, 12-27.

Audetat, A., Pettke, T., Heinrich, C.A., Bodnar, R.J., 2008. The Composition of Magmatic-Hydrothermal Fluids in Barren and Mineralized Intrusions. Economic Geology 103, 877-908.

Baker, T., Mustard, R., Fu, B., Williams, P.J., Dong, G.Y., Fisher, L., Mark, G., Ryan, C.G., 2008. Mixed messages in iron oxide-copper-gold systems of the Cloncurry district, Australia: insights from PIXE analysis of halogens and copper in fluid inclusions. Mineralium Deposita 43, 599-608.

Balcone-Boissard, H., Villemant, B., Boudon, G., 2010. Behavior of halogens during the degassing of felsic magmas. Geochemistry Geophysics Geosystems 11.

Berndt, M.E., Seyfried, W.E., 1997. Calibration of Br/Cl fractionation during subcritical phase separation of seawater: Possible halite at 9 to 10 degrees N East Pacific Rise. Geochimica et Cosmochimica Acta 61, 2849-2854.

Bischoff, J.L., Rosenbauer, R.J., Fournier, R.O., 1996. The generation of HCl in the system $CaCl_2$-H2O: Vapor-liquid relations from 380-500 °C. Geochimica et Cosmochimica Acta 60, 7-16.

Bodnar, R.J., Burnham, C.W., Sterner, S.M., 1985. Synthetic fluid inclusions in natural quartz. 3. Determination of phase-equilibrium properties in the system H_2O-NaCl to 1000°C and 1500 bars. Geochimica et Cosmochimica Acta 49, 1861-1873.

Bohlke, J.K., Irwin, J.J., 1992a. Brine history indicated by argon, krypton, chlorine, bromine, and iodine analyses of fluid inclusions from the Mississippi Valley type lead fluorite barite deposits ar Hansonburg, New-Mexico. Earth and Planetary Science Letters 110, 51-66.

Bohlke, J.K., Irwin, J.J., 1992b. Laser microprobe analyese of noble-gas isotopes and halogens in fluid inclusions - Analyses of microstandards and synthetic inclusions in quartz. Geochimica et Cosmochimica Acta 56, 187-201.

Braitsch, O., 1971. Salt deposits; their origin and composition. Springer-Verlag.

Bray, C.J., Spooner, E.T.C., 1992. Fluid inclusion volatile analysis by gas-chromatography with photoionization micro-thermal conductivity detectors - applications to magmatic MoS_2 and other H_2O-CO_2 and H_2O-CH_4 fluids. Geochimica et Cosmochimica Acta 56, 261-272.

Channer, D.M.D., de Ronde, C.E.J., Spooner, E.T.C., 1997. The Cl^- – Br^- – I^- composition of ~3.23 Ga modified seawater: implications for the geological evolution of ocean halide chemistry. Earth and Planetary Science Letters 150, 325-335.

Driesner, T., Heinrich, C.A., 2007. The system H_2O-NaCl. Part I: Correlation formulae for phase relations in temperature-pressure-composition space from 0 to 1000 °C, 0 to 5000 bar, and 0 to 1 X-NaCl. Geochimica et Cosmochimica Acta 71, 4880-4901.

Dubois, M., Weisbrod, A., Shtuka, A., 1994. Experimental determination of the 2-phase (liquid and vapor) region in water alkali chloride binary-system at 500 °C and 600 °C using synthetic fluid inclusions. Chemical Geology 115, 227-238.

Foriel, J., Philippot, P., Rey, P., Somogyi, A., Banks, D., Menez, B., 2004. Biological control of Cl/Br and low sulfate concentration in a 3.5-Gyr-old seawater from North Pole, Western Australia. Earth and Planetary Science Letters 228, 451-463.

Fournier, R.O., 1987. Conceptual models of brine evolution in magmatic-hydrothermal systems, in: Decker, R.W., Wright, T.L., Stauffer, P.H. (Eds.), Professional Paper 1350. US Geological Survey, pp. 1487-1506.

Fournier, R.O., Thompson, J.M., 1993. Composition of steam in the system NaCl-KCl-H_2O-quartz at 600 °C. Geochimica et Cosmochimica Acta 57, 4365-4375.

Foustoukos, D.I., Seyfried, W.E., 2007. Trace element partitioning between vapor, brine and halite under extreme phase separation conditions. Geochimica et Cosmochimica Acta 71, 2056-2071.

Günther, D., Frischknecht, R., Heinrich, C.A., Kahlert, H.J., 1997. Capabilities of an Argon Fluoride 193 nm excimer laser for laser ablation inductively coupled plasma mass spectrometry microanalysis of geological materials. Journal of Analytical Atomic Spectrometry 12, 939-944.

Gleeson, S.A., Wilkinson, J.J., Stuart, F.M., Banks, D.A., 2001. The origin and evolution of base metal mineralising brines and hydrothermal fluids, South Cornwall, UK. Geochimica Et Cosmochimica Acta 65, 2067-2079.

Gleeson, S.A., Smith, M.P., 2009. The sources and evolution of mineralising fluids in iron oxide-copper-gold systems, Norrbotten, Sweden: Constraints from Br/Cl ratios and stable Cl isotopes of fluid inclusion leachates. Geochimica et Cosmochimica Acta 73, 5658-5672.

Gruszkiewicz, M.S., Wood, R.H., 1997. Conductance of dilute LiCl, NaCl, NaBr, and CsBr solutions in supercritical water using a flow conductance cell. J. Phys. Chem. B 101, 6549-6559.

Guillong, M., Heinrich, C.A., 2007. Sensitivity enhancement in laser ablation ICP-MS using small amounts of hydrogen in the carrier gas. Journal of Analytical Atomic Spectrometry 22, 1488-1494.

Guillong, M., Latkoczy, C., Seo, J.H., Günther, D., Heinrich, C.A., 2008. Determination of sulfur in fluid inclusions by laser ablation ICP-MS. Journal of Analytical Atomic Spectrometry 23, 1581-1589.

Heijlen, W., Muchez, P., Banks, D.A., Schneider, J., Kuchia, H., Keppens, E., 2003. Carbonate-hosted Zn-Pb deposits in Upper Silesia, Poland: Origin and evolution of mineralizing fluids and constraints on genetic models. Economic Geology 98, 911-932.

Heinrich, C.A., Bain, J.H.C., Fardy, J.J., Waring, C.L., 1993. Br/Cl geochemistry of hydrothermal brines associated with Proterozoic metasediment-hosted copper mineralization at Mount Isa, northwestern Australia. Geochimica et Cosmochimica Acta 57, 2991-3000.

Heinrich, C.A., Pettke, T., Halter, W.E., Aigner-Torres, M., Audétat, A., Günther, D., Hattendorf, B., Bleiner, D., Guillong, M., Horn, I., 2003. Quantitative multi-element analysis of minerals, fluid and melt inclusions by laser-ablation inductively-coupled-plasma mass-spectrometry. Geochimica et Cosmochimica Acta 67, 3473-3497.

Heinrich, W., 2007. Fluid immiscibility in metamorphic rocks, in: Liebscher, A., Heinrich, C.A.

(Eds.), Fluid-Fluid Interactions, pp. 389-430.

Ho, P.C., Palmer, D.A., Mesmer, R.E., 1994. Electrical-conductivity measurements of aqueous sodium-chloride solutions to 600 °C and 300 MPa. Journal of Solution Chemistry 23, 997-1018.

Ho, P.C., Palmer, D.A., 1996. Ion association of dilute aqueous sodium hydroxide solutions to 600 °C and 300 MPa by conductance measurements. Journal of Solution Chemistry 25, 711-729.

Ho, P.C., Palmer, D.A., 1997. Ion association of dilute aqueous potassium chloride and potassium hydroxide solutions to 600 °C and 300 MPa determined by electrical conductance measurements. Geochimica et Cosmochimica Acta 61, 3027-3040.

Ho, P.C., Palmer, D.A., 1998. Determination of ion association in dilute aqueous lithium chloride and lithium hydroxide solutions to 600 °C and 300 MPa by electrical conductance measurements. Journal of Chemical and Engineering Data 43, 162-170.

Ho, P.C., Bianchi, H., Palmer, D.A., Wood, R.H., 2000a. Conductivity of dilute aqueous electrolyte solutions at high temperatures and pressures using a flow cell. Journal of Solution Chemistry 29, 217-235.

Ho, P.C., Palmer, D.A., Wood, R.H., 2000b. Conductivity measurements of dilute aqueous LiOH, NaOH, and KOH solutions to high temperatures and pressures using a flow-through cell. J. Phys. Chem. B 104, 12084-12089.

Hovey, J.K., Pitzer, K.S., Tanger, J.C., Bischoff, J.L., Rosenbauer, R.J., 1990. Vapor-liquid phase equilibria of potassium chloride-water mixtures: equation-of-state representation for potassium chloride-water and sodium chloride-water. Journal of Physical Chemistry 94, 1175-1179.

Jolly, W.L., 1984. Modern Inorganic Chemistry. McGraw-Hill, New York.

Kesler, S.E., Appold, M.S., Martini, A.M., Walter, L.M., Huston, T.J., Kyle, J.R., 1995. Na-Cl-Br systematics of mineralizing brines in Mississippi Valley-type deposits. Geology 23, 641-644.

Kesler, S.E., Martini, A.M., Appold, M.S., Walter, L.M., Huston, T.J., Furman, F.C., 1996. Na-Cl-Br systematics of fluid inclusions from Mississippi valley-type deposits, Appalachian basin: Constraints on solute origin and migration paths. Geochimica et Cosmochimica Acta 60, 225-233.

Klemm, L.M., Pettke, T., Heinrich, C.A., Campos, E., 2007. Hydrothermal evolution of the El Teniente deposit, Chile: Porphyry Cu-Mo ore deposition from low-salinity magmatic fluids. Economic Geology 102, 1021-1045.

Kouzmanov, K., Pokrovski, G.S., 2012. Hydrothermal Controls on Metal Distribution in Porphyry Cu (-Mo-Au) Systems. Society of Economic Geologist Special Publication 16, 573-618.

Lesne, P., Kohn, S.C., Blundy, J., Witham, F., Botcharnikov, R.E., Behrens, H., 2011. Experimental Simulation of Closed-System Degassing in the System Basalt-H2O-CO2-S-Cl. Journal of Petrology 52, 1737-1762.

Liebscher, A., Luders, V., Heinrich, W., Schettler, G., 2006. Br/Cl signature of hydrothermal fluids: liquid-vapour fractionation of bromine revisited. Geofluids 6, 113-121.

Liebscher, A., 2007. Experimental studies in model fluid systems, in: Liebscher, A., Heinrich, C.A. (Eds.), Fluid-Fluid Interactions, pp. 15-47.

Liebscher, A., Meixner, A., Romer, R.L., Heinrich, W., 2007. Experimental calibration of the vapour-liquid phase relations and lithium isotope fractionation in the system H_2O-LiCl at 400 °C/20-28 MPa. Geofluids 7, 369-375.

Muchez, P., Heijlen, W., Banks, D., Blundell, D., Boni, M., Grandia, F., 2005. Extensional tectonics and the timing and formation of basin-hosted deposits in Europe. Ore Geology Reviews 27, 241-267.

Nahnybida, T., Gleeson, S.A., Rusk, B.G., Wassenaar, L.I., 2009. Cl/Br ratios and stable chlorine isotope analysis of magmatic-hydrothermal fluid inclusions from Butte, Montana and Bingham Canyon, Utah. Mineralium Deposita 44, 837-848.

Oosting, S.E., Von Damm, K.L., 1996. Bromide/chloride fractionation in seafloor hydrothermal fluids from 9-10 degrees N east Pacific rise. Earth and Planetary Science Letters 144, 133-145.

Palmer, D.A., Simonson, J.M., Jensen, J.P., 2004. Partitioning of electrolytes to steam and their solubilities in steam., in: Palmer, D.A., Fernandez-Prini, R., Harvey, A.H. (Eds.), Aqueous Systems at Elevated Temperatures and Pressures: Physical Chemistry in Water, Steam and Hydrothermal Solutions. Elsevier, pp. 407-439.

Roedder, E., 1984. Fluid inclusions. Reviews in Mineralogy 12, 1-&.

Seo, J.H., Guillong, M., Aerts, M., Zajacz, Z., Heinrich, C.A., 2011. Microanalysis of S, Cl, and Br in fluid inclusions by LA-ICP-MS. Chemical Geology 284, 35-44.

Shannon, R.D., 1976. Revised effective ionic radii and systematic studies of interatomic distances in halides and chalcogenides. Acta Crystallographica Section A A32, 751-767.

Shmulovich, K.I., Tkachenko, S.I., Plyasunova, N.V., 1995. Phase equilibria in fluid systems at high pressures and temperatures, in: Shmulovich, K.I., Yardley, B.W.D., Gonchar, G.G. (Eds.), Fluids in the Crust. Springer Netherlands, pp. 193-214.

Sterner, S.M., Bodnar, R.J., 1984. Synthetic fluid inclusions in natural quartz I. Compositional types synthesized and applications to experimental geochemistry. Geochimica et Cosmochimica Acta 48, 2659-2668.

Stoffell, B., Appold, M.S., Wilkinson, J.J., McClean, N.A., Jeffries, T.E., 2008. Geochemistry and Evolution of Mississippi Valley-Type Mineralizing Brines from the Tri-State and Northern Arkansas Districts Determined by LA-ICP-MS Microanalysis of Fluid Inclusions. Economic Geology 103, 1411-1435.

Urusova, M.A., 1974. Phase equilibria in the sodium hydroxide-water and sodium chloride-water systems at 350-550 °C. Russ. J. Inorg. Chem. 19, 450-454.

Von Damm, K.L., Lilley, M.D., Shanks, W.C., Brockington, M., Bray, A.M., O'Grady, K.M., Olson, E., Graham, A., Proskurowski, G., Sou, E.P.R.S.P., 2003. Extraordinary phase separation and segregation in vent fluids from the southern East Pacific Rise. Earth and Planetary Science Letters 206, 365-378.

Wilkinson, J.J., Everett, C.E., Boyce, A.J., Gleeson, S.A., Rye, D.M., 2005. Intracratonic crustal seawater circulation and the genesis of subseafloor zinc-lead mineralization in the Irish orefield. Geology 33, 805-808.

Williams-Jones, A.E., Migdisov, A.A., Archibald, S.M., Xiao, Z., 2002. Vapor transport of ore metals, in: Hellmann, R., Wood, S.A. (Eds.), Water-rock interations, Ore Deposits, and Environmental Geochemistry: A Tribute to David A. Crerar. The Geochemical Society, pp. 279-305.

Williams, T.J., Candela, P.A., Piccoli, P.M., 1997. Hydrogen-alkali exchange between silicate melts and two-phase aqueous mixtures: an experimental investigation. Contributions to Mineralogy and Petrology 128, 114-126.

Yardley, B.W.D., 2005. Metal concentrations in crustal fluids and their relationship to ore formation. Economic Geology 100, 613-632.

.